Decomposition and Vibrational Relaxation in CH_3I and Self-Reaction of CH_3 Radicals

Xueliang Yang,[†] C. Franklin Goldsmith,[‡] and Robert S. Tranter*,[†]

Chemical Sciences and Engineering Division, Argonne National Laboratory, 9700 South Cass Avenue, Argonne, Illinois 60439, and Department of Chemical Engineering, Massachusetts Institute of Technology, 77 Massachusetts Avenue, Cambridge, Massachusetts 02139-4307

Received: April 10, 2009; Revised Manuscript Received: May 22, 2009

Vibrational relaxation and dissociation of CH_3I, 2−20% in krypton, have been investigated behind incident shock waves in a diaphragmless shock tube at 20, 66, 148, and 280 Torr and 630−2200 K by laser schlieren densitometry. The effective collision energy obtained from the vibrational relaxation experiments has a small, positive temperature dependence, $\langle\Delta E\rangle_{down} = 63 \times (T/298)^{0.56}$ cm^{-1}. First-order rate coefficients for dissociation of CH_3I show a strong pressure dependence and are close to the low-pressure limit. Restricted-rotor Gorin model RRKM calculations fit the experimental results very well with $\langle\Delta E\rangle_{down} = 378 \times (T/298)^{0.457}$ cm^{-1}. The secondary chemistry of this reaction system is dominated by reactions of methyl radicals and the reaction of the H atom with CH_3I. The results of the decomposition experiments are very well simulated with a model that incorporates methyl recombination and reactions of methylene. Second-order rate coefficients for ethane dissociation to two methyl radicals were derived from the experiments and yield $k = (4.50 \pm 0.50) \times 10^{17}$ exp(−32709/T) cm^3 mol^{-1} s^{-1}, in good agreement with previous measurements. Rate coefficients for H + CH_3I were also obtained and give $k = (7.50 \pm 1.0) \times 10^{13}$ exp(−601/T) cm^3 mol^{-1} s^{-1}, in reasonable agreement with a previous experimental value.

Introduction

Methyl iodide is potentially a clean, thermal, high-temperature source of CH_3 radicals for shock tube experiments because it dissociates solely by fission of the C−I bond[1−6] and the I atom is essentially inactive.

$$CH_3I + M \rightarrow CH_3 + I + M \quad (1)$$

Consequently, reaction 1 could be an effective method of generating CH_3 radicals to study their recombination reactions and reactions with other species. However, methyl radicals are reactive, and unless their subsequent reactions are effectively suppressed, secondary chemistry may limit the usefulness of CH_3I as a precursor. Prior shock tube, ST, experiments that either investigated the dissociation of methyl iodide or used it as a CH_3 source were performed with I-ARAS[1,6] (atomic resonance absorption spectroscopy), CH_3 ultraviolet (UV) absorption,[4,5,7] or CH_3I UV absorption[2,3] and were conducted with low reagent concentrations, <0.02%, which minimized secondary reactions. Techniques such as ST/TOF-MS (time-of-flight mass spectrometry) and ST/LS (laser schlieren densitometry) typically require initial reagent concentrations in the 0.5−5% range, and even at quite low reaction pressures, secondary chemistry can be expected to be quite significant and must be accounted for when determining the concentrations of reactive species such as CH_3. Thus, prior to using methyl iodide as a source of methyl radicals, as is our intent, it is necessary to fully characterize the dissociation reaction, reaction 1, and secondary chemistry over the range of anticipated reaction conditions.

As well as the shock tube investigations mentioned above, the decomposition of CH_3I has also been studied in static reactors[8,9] and flow reactors[10,11] with a variety of diagnostics. The high-temperature second-order rate coefficients for reaction 1 from Takahashi et al.[1] and Kumaran et al.[6] are in excellent agreement, and they used argon and krypton, respectively, as bath gases. The measurements of Davidson et al.,[4] argon bath gas, lie about 30% higher than Kumaran et al. and have an activation energy of around 30% lower. The data of Baeck et al.[5] have an activation energy that is about 35% lower than that of Kumaran et al. but a smaller A factor, and the two data sets cross at about 1470 K. The results of Saito et al.[2,3] are lower than these by factors of 3 and 6 for argon and krypton bath gases, respectively. While differences in the rate expressions exist, all of the previous studies agree that the sole initial reaction for CH_3I pyrolysis is reaction 1 and that there is no evidence for HI elimination.

In experiments where the reagent concentrations are sufficient to promote secondary chemistry, a complex chain process initiated by the methyl−methyl self-reaction can be anticipated. This alkyl radical recombination has four channels, reactions 2−5, which have been investigated to varying degrees.

$$CH_3 + CH_3 + M \rightarrow C_2H_6 + M \quad (2)$$

$$CH_3 + CH_3 \rightarrow C_2H_5 + H \quad (3)$$

$$CH_3 + CH_3 \rightarrow {}^3CH_2 + CH_4 \quad (4)$$

$$CH_3 + CH_3 \rightarrow {}^1CH_2 + CH_4 \quad (5)$$

Reaction 2 and its reverse reaction have been examined experimentally and theoretically in studies too numerous to cite,

* To whom correspondence should be addressed. E-mail: tranter@anl.gov.
[†] Argonne National Laboratory.
[‡] Massachusetts Institute of Technology.

10.1021/jp903336u CCC: $40.75
Published on Web 07/01/2009

and the reader is referred to the NIST kinetics database[12] for a comprehensive list that includes several critical evaluations. The most recent experimental reports concerning reaction 2 at temperatures and pressures close to the current work are a ST/LS study of the reverse of reaction 2, reaction −2,[13] and a ST/UV absorption study also of reaction −2, which monitored CH_3 production.[14] The results of the two studies are in good agreement and the experimental rate coefficients, k_{-2}, are in good agreement with master equation (M.E.) calculations.[13] Kiefer et al. also proposed a high-temperature model for ethane dissociation, and this model may be expected to describe the CH_3-initiated secondary reactions adequately in this study of CH_3I dissociation at similar conditions, $1400 < T < 2200$ K and $70 < P < 5700$ Torr, and the same diagnostic, LS ($P < 500$ Torr), were used as in the current work.

Reaction 3 has been investigated at high temperatures in several shock tube studies.[7,15−18] Frank and Braun-Unkhoff[17] and Lim and Michael[15] used H-ARAS to monitor the reaction directly and obtained results that are within 20% of each other. A more indirect estimation of the rate coefficient has been made by Davidson et al.[7] and is in good agreement with the ARAS work.

The literature data for reactions 4 and 5 are considerably more limited. They have been experimentally studied at low temperature by Bohland et al.,[19] and while they are unlikely to contribute significantly to the removal of CH_3 radicals compared to reactions 2 and 3, the products, $^3CH_2$ and $^1CH_2$, are reactive,[7,20] and subsequent reactions are likely to be important.

At sufficiently low reaction pressures, the rather sparse vibrational-state density in methyl iodide suggests that vibrational relaxation in the molecule should be observable with ST/LS, and incubation delays may be significant in the dissociation studies. As has been previously demonstrated, LS is particularly well suited to the study of incubation and vibrational relaxation at elevated temperatures; see, for example, refs 21−23.

Given the above considerations, to use reaction 1 as a source of CH_3 radicals in relatively high concentration reaction environments, dissociation of CH_3I needs to be thoroughly investigated, and the effects of incubation need to be considered. Consequently, a series of experiments have been performed using ST/LS to investigate not only the dissociation reaction but the associated secondary chemistry due to methyl self-reaction. Furthermore, the current studies incorporate investigation of relaxation and incubation in CH_3I/Kr mixtures at elevated temperatures and low pressures. These additional results have been used in conjunction with pure dissociation experiments to develop a model for the high-temperature self-reaction of methyl radicals.

Experimental Section

The LS experiments were performed in a diaphragmless shock tube, DFST, for which the operation and characteristics have been fully described elsewhere.[24] The driver section of the DFST contains a fast-acting valve which replaces the more traditional diaphragm. When the valve is closed, the driver and driven sections can be filled to the desired loading pressures, and the DFST is fired by rapidly opening the valve. By varying both the driver section pressure, P_4, and the driven section pressure, P_1, the pressure behind the incident shock wave, P_2, can be constrained to very narrow ranges,[24] typically $<\pm 3\%$, over a wide range of temperatures.

The driven section of the shock tube has an internal diameter of 7.012 cm, and the quartz windows through which the beam from a helium−neon laser passes for LS measurements are located sufficiently far downstream to allow the shock wave to be fully developed after firing the DFST. A set of six pressure transducers evenly spaced along the side of the driven section are centered around the LS windows, and incident shock wave velocities are obtained by interpolation of the five intervals calculated from the measured times taken for the shock wave to arrive at successive pressure transducers. From these velocities and the loading conditions, the temperature and pressure behind the incident shock wave are calculated assuming frozen conditions. The uncertainty in velocity is estimated as 0.2%, corresponding to a temperature error of less than 0.5%, here amounting to the order of 10−15 K.

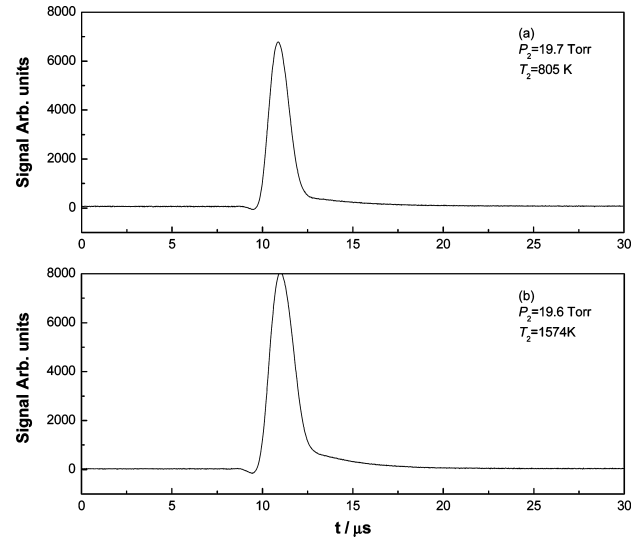

Figure 1. Example laser schlieren profiles showing vibrational relaxation in (a) 10 and (b) 20% CH_3I/Kr mixtures.

The LS diagnostics have also been described previously, and a similar configuration to that of Kiefer et al.[25,26] is used with the only significant difference being the use of a 14-bit Compuscope 14100 data acquisition card (GAGE Applied Electronics) in place of a 12-bit data acquisition card. The molar refractivity of Kr = 6.367 was taken from Gardiner et al.,[27] and that of CH_3I = 19.25 was calculated from its refractive index, 1.53, and molar density, 2.28 cm^3/mol, at 20 °C. As usual, the reasonable assumption that changes in the mixture refractive index are negligible throughout the course of reaction[25] is made.

Regent Mixtures. Mixtures of CH_3I dilute in krypton were prepared manometrically in a 50 L glass vessel that had been evacuated to $<10^{-3}$ Torr. Krypton (AGA 99.999%), was used as supplied. CH_3I (Aldrich Chemical Co., 99%) was degassed by repeated freeze−pump−thaw cycles with liquid nitrogen before use. Mixtures containing 2 and 4% CH_3I were prepared for dissociation experiments, and mixtures of 2, 10, and 20% were prepared for the vibrational relaxation experiments. The mixture compositions had uncertainties of less than ±0.1% and were allowed to homogenize for several hours prior to use.

Results and Discussion

Vibrational Relaxation. Vibrational relaxation in methyl iodide was observed over a temperature range of 636−1686 K in mixtures of 2, 10, and 20% CH_3I in Kr at post shock pressures of 20 ± 1 Torr in 56 experiments. The postshock temperature and pressure, T_2 and P_2, respectively, were calculated assuming the fully relaxed condition. Typical raw LS profiles from two experiments are shown in Figure 1. The large spike and preceding valley are from interaction of the shock front with

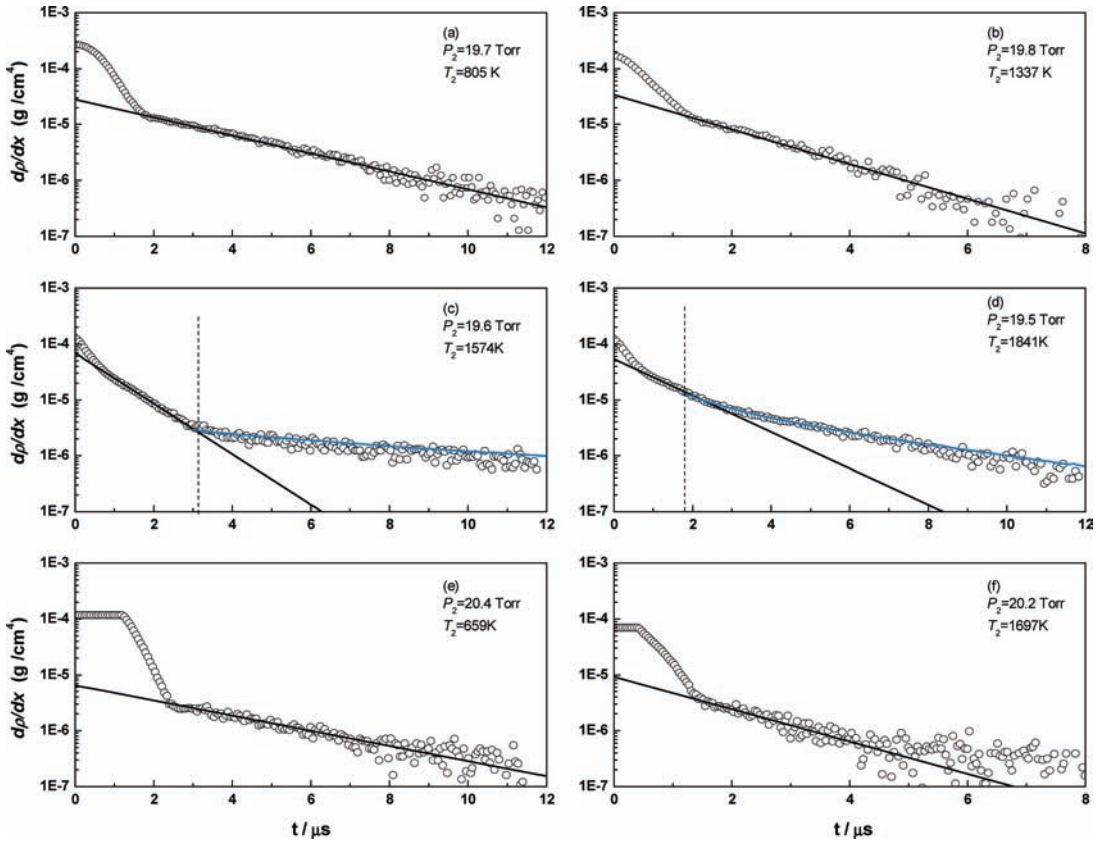

Figure 2. Example semilog plots of density gradients for vibrational relaxation in (a and b) 10, (c and d) 20, and (e and f) 2% CH_3I/Kr mixtures. The open circles (○) are experimental measurements, the solid lines are linear fits to the exponential signal due to relaxation, and the blue dashed lines are the results of simulations using the mechanism listed in Table 1. The vertical dotted lines indicate the switch from relaxation to dissociation and are used to mark incubation periods. See text for a discussion of relaxation and incubation in experiments similar to (d).

the laser beam. The signal prior to arrival of the shock wave at the observation station is used to establish a baseline in each experiment. At around 12 μs (Figure 1) there is a sharp change in the signal, and the remainder of the data represents the signal of interest. Semilog plots of density gradients that are derived from the raw LS signals are presented in Figure 2. The raw data shown in Figure 1a and b correspond to the density gradient profiles presented in Figure 2a and b. The initial few, steeply falling points in each plot of Figure 2 are from the tail of the shock front/laser beam interaction in Figure 1.

The density gradients obtained from the 20 Torr experiments are very closely exponential in all cases for $T_2 < 1400$ K, Figure 2a, b, and e indicating that the signal is due to pure relaxation with no contribution from the dissociation of CH_3I. For $T_2 >$ 1400 K, in experiments with 10 and 20% methyl iodide, dissociation of CH_3I begins to contribute to the density gradient profiles, and for a number of experiments, a two-stage decay pattern with the first part being exponential is clearly observed, from which a measure of incubation time can also be obtained. An example two-stage profile is shown in Figure 2c, where the solid line indicates the initial relaxation, the blue solid line represents simulation of the dissociation process using the mechanism in Table 1, and the vertical dashed line indicates the start of dissociation and hence gives a measure of incubation time. Above 1700 K, the relaxation time is very short, and it is difficult to distinguish relaxation from dissociation and obtain an accurate estimate of the relaxation time, as shown in Figure 2d, where the transition from relaxation to dissociation is not clearly defined. As well, as the greater contribution of dissociation to the density gradient, the heat capacities of the 10 and 20% mixtures are quite large, which results in a large time compression[22] between laboratory and molecule time through the increased density ratio across the shock front. In these experiments, the net effect is to make resolution of relaxation in high concentration mixtures at high temperatures difficult. However, in the lower concentration, 2%, experiments relaxation can be resolved to much higher temperatures. For example, Figure 2f contains the density gradient plot for an experiment with 2% CH_3I and $T_2 = 1697$ K, and the density gradients are clearly exponential over the first 4 μs. The latter part of the signal may show traces of dissociation, but the density gradients are very small, and accurate assignment is difficult. Furthermore, it should be noted that the density gradients found in the 2% experiments are about an order of magnitude smaller than those from the 20% experiments. Apparent relaxation times, τ_{app}, were readily derived from the early linear portion of the semilog LS profiles and converted to the vibrational energy relaxation time, $P\tau$,[28] using the Bethe−Teller approximation as specified by Blythe,[29] similar to previous LS studies of vibrational relaxation at high temperature.[30]

The vibrationally relaxed conditions and derived $P\tau$ are shown in a Landau−Teller plot, Figure 3, and are available in the electronic Supporting Information. The relaxation times decrease steadily with increasing temperature, indicating that the collision energy is increasing with the temperature. Above 1600 K, there is an increase in $P\tau$ in the 10% and 20% experiments that is not observed in the more dilute 2% experiments. Fogg et al.[31] estimated the relaxation time in pure CH_3I at 373 K to be about 180 ns atm (Figure 3).

From each of the measured $P\tau$, an effective $\langle \Delta E \rangle_{down}$ has been calculated which excludes the vibrational energy and the collision frequency effects from the problem.[32] The calculation

TABLE 1: Reaction Mechanism and Arrhenius Parameters for Methyl Iodide Pyrolysis[a]

	reaction	log *A*	*n*	E_a	$\Delta H_{r,298}$	reaction in ref 13	source
R_1	$CH_3I + M = CH_3 + I + M$	35.600	−5.40	58.300	57.1		this work
R_2	$C_2H_6 + M = CH_3 + CH_3 + M$	18.250	0.00	69.996	90.2	1	this work
R_3	$CH_3 + CH_3 = C_2H_5 + H$	13.732	0.00	16.055	10.6	4	15
R_4	$CH_4 + CH_2$ (T) $= CH_3 + CH_3$	6.390	2.00	8.270	−5.5		7
R_5	CH_2 (S) $+ CH_4 = CH_3 + CH_3$	13.204	0.00	−0.570	−14.5		7
R_6	$C_2H_4 + H = C_2H_5$	43.025	−9.28	13.974	−36.0	5	41
R_7	$H + CH_3I = CH_3 + HI$	13.877	0.00	1.195	−14.2		this work
R_8	$C_2H_6 + H = C_2H_5 + H_2$	2.740	3.50	5.167	−3.5	2	37
R_9	$C_2H_6 + CH_3 = C_2H_5 + CH_4$	−0.261	4.00	8.286	−4.3	3	13
R_{10}	$C_2H_4 + H = C_2H_3 + H_2$	7.703	1.93	12.951	6.2	6	42
R_{11}	$CH_4 + M = CH_3 + H + M$	47.219	−8.00	121.470	105.0	7	43
R_{12}	$C_2H_4 + M = C_2H_2 + H_2 + M$	17.310	0.00	78.271	42.0	8	42
R_{13}	$C_2H_4 + M = C_2H_3 + H + M$	17.413	0.00	96.580	110.4	9	42
R_{14}	$C_2H_5 + H = C_2H_4 + H_2$	12.300	0.00	0.000	−68.2	10	7
R_{15}	$C_2H_2 + H = C_2H_3$	31.079	−6.1	6.476	−35.8	11	41
R_{16}	$C_2H_3 + H = C_2H_2 + H_2$	13.600	0.00	0.000	−68.4	12	42
R_{17}	$CH_4 + H = CH_3 + H_2$	5.778	2.50	9.650	0.8	13	43
R_{18}	CH_2(T) $+ CH_3 = C_2H_4 + H$	15.070	−0.34	−0.153	−63.9		20
R_{19}	CH_2 (S) $+ H_2 = H + CH_3$	13.800	0.00	0.000	−15.3		42
R_{20}	$CH_3 + M = CH_2$ (T) $+ H + M$	16.000	0.00	90.611	110.5		42
R_{21}	$C_3H_8 + M = CH_3 + C_2H_5 + M$	18.892	0.00	64.945	88.7		44
R_{22}	$CH_3 + C_2H_5 = C_2H_4 + CH_4$	11.950	0.00	0.000	−69.0		42
R_{23}	$H + H + M = H_2 + M$	18.000	−1.00	0.000	−104.2		42
R_{24}	$C_2H_6 = H + C_2H_5$	42.488	−7.93	111.000	100.8		16
R_{25}	CH_2 (S) $+ CH_3 = C_2H_4 + H$	13.079	0.00	−0.570	−72.8		7
R_{26}	CH_2 (S) $+ M = CH_2$ (T) $+M$	12.950	0.00	0.600	−9.0		7
R_{27}	CH_2 (S) $+ C_2H_6 = CH_3 + C_2H_5$	13.600	0.00	−0.550	−18.8		7
R_{28}	CH_2 (T) $+ CH_2$ (T) $= C_2H_2 + H_2$	13.500	0.00	0.000	−132.5		7
R_{29}	CH_2 (T) $+ H_2 = H + CH_3$	5.700	2.00	7.230	−6.3		7
R_{30}	$CH_3 + CH_3I = CH_2$(T) $+ CH_4 + I$	12.100	0.00	12.100	62.63		45
R_{31}	$CH + H_2 = H + CH_2$(T)	14.500	0.00	3.100	3.20		7
R_{32}	$CH + CH_2$(T) $= H + C_2H_2$	13.600	0.00	0.000	−129.26		7
R_{33}	$CH + CH_3 = H + C_2H_3$	13.500	0.00	0.000	−54.48		7
R_{34}	$CH + CH_4 = H + C_2H_4$	13.800	0.00	0.000	−59.87		7

[a] Pressure-dependent rate coefficients in the table are for 280 Torr. Units: kcal/mol cm^3 mol s.

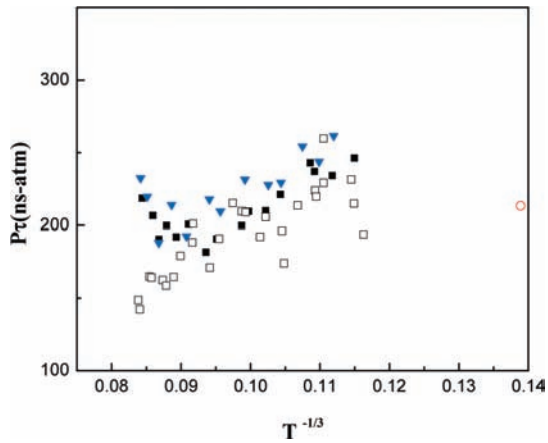

Figure 3. Landau−Teller plot of vibrational relaxation times for [■] 20, [blue ▼] 10, and [□] 2% CH_3I/Kr at 20 Torr. [Red ○] is the vibrational relaxation time of pure CH_3I calculated from Fogg et al.[31] at 373 K.

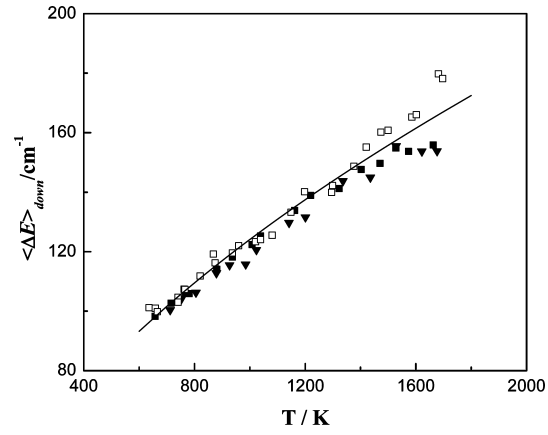

Figure 4. Values for $\langle\Delta E\rangle_{down}$ derived from relaxation times for [■] 20, [blue ▼] 10, and [□] 2% CH_3I/Kr at 20 Torr. The solid line is the linear least-squares fit and gives $\langle\Delta E\rangle_{down} = 63 \times (T/298)^{0.56}$.

of $\langle\Delta E\rangle_{down}$, initially assumed that the Landau−Teller selection was dominant and only single quantum jumps were permitted. The assumption was validated by also estimating $\langle\Delta E\rangle_{down}$ allowing all transitions, and negligible change was found. These calculated $\langle\Delta E\rangle_{down}$ are shown in Figure 4, and a fit to the data, excluding the 10 and 20% points above 1600 K, gives $\langle\Delta E\rangle_{down} = (63 \pm 3) \times (T/298)^{0.56}$. Clearly, up to 1600 K, the $\langle\Delta E\rangle_{down}$ obtained for 10 and 20% mixtures are in good agreement with those from the 2% experiments. The remaining few high-temperature points for the 10 and 20% experiments abruptly flatten out and show no further increase, whereas the 2% results follow the same increasing trend. We suggest that in the higher-temperature 10 and 20% experiments, dissociation of CH_3I is contributing significantly to the early portion of the density gradient profile and that relaxation can no longer be distinguished from dissociation, and thus, the apparent relaxation gradients are in fact combinations of the two effects. This can be seen in Figure 2d, where there is no clear break between relaxation and dissociation, unlike that seen in Figure 2c, and in fact, the assignment of the onset of dissociation in Figure 2d is really quite arbitrary. Conversely, in the 2% experiments, the density gradients remain exponential to at least 1600 K, Figure

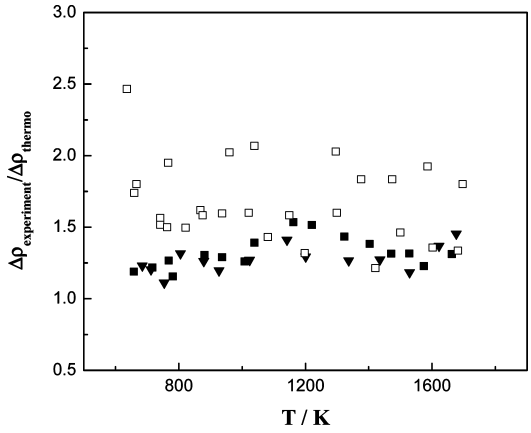

Figure 5. The $\Delta\rho_{experiment}/\Delta\rho_{thermo}$ for [■] 20, [blue ▼] 10, and [□] 2% CH_3I/Kr at 20 ± 1 Torr.

2f, with only faint indications of dissociation at long times for $T > 1600$ K.

Calculated thermodynamic and experimental density changes upon relaxation, $\Delta\rho = \rho(\infty) - \rho(0)$, the difference between fully relaxed, $\rho(\infty)$, and unrelaxed, $\rho(0)$, post shock densities are shown in Figure 5 and are available in Table 1 of the Supporting Information. When the density gradients are accurately exponential as in the present experiments, the experimental $\Delta\rho$ can be obtained by integration of the density gradient.[30] The τ_{app} and $(d\rho/dx)_{t=0}$, the density gradient at t_0, are obtained directly from plots similar to those in Figure 2, and u_1 is the incident shock velocity.

$$\Delta\rho = u_1 \int_0^\infty \left(\frac{d\rho}{dx}\right)_{t=0} \exp(-t/\tau_{app})dt = u_1\tau_{app}\left(\frac{d\rho}{dx}\right)_{t=0}$$

In principle, the ratio of experimental to thermodynamic $\Delta\rho$ values should be close to unity, especially for the experiments at low temperatures. These are plotted in Figure 5 and generally lie around 1.3 for the 10 and 20% experiments, indicating that the estimation of the relaxation times is reasonably accurate. There is greater scatter in the results from the 2% experiments, centered at around 1.5, than in the 10 and 20% data, which is due in part to the weaker signals giving greater uncertainty in the density gradient at t_0.

Incubation. The incubation times for the onset of steady-state dissociation are typically some small multiples of the relaxation time,[32] and they are important factors for the determination of rate coefficients for the dissociation of CH_3I, R_1 (R_x refers to reaction numbers in Table 1), from the experimental results. As discussed above, it was possible in a number of low-pressure experiments to obtain estimates of the incubation times, t_{inc}, and these vary from 1.5 to 3 μs.

Dissociation of CH_3I. A total of 108 experiments on CH_3I pyrolysis were carried out for incident shock pressures of 66 ± 2, 146 ± 4, and 280 ± 6 Torr and incident shock temperatures of 1490−2181 K. Example raw LS profiles are shown in Figure 6, and the corresponding semilog density gradient plots are shown in Figure 7. As in the vibrational relaxation work, the initial valley and large spike in each plot of Figure 6 are due to shock front/laser beam interaction. Figure 6a and b looks superficially similar to the examples of vibrational relaxation experiments shown in Figure 2, but in these experiments, the

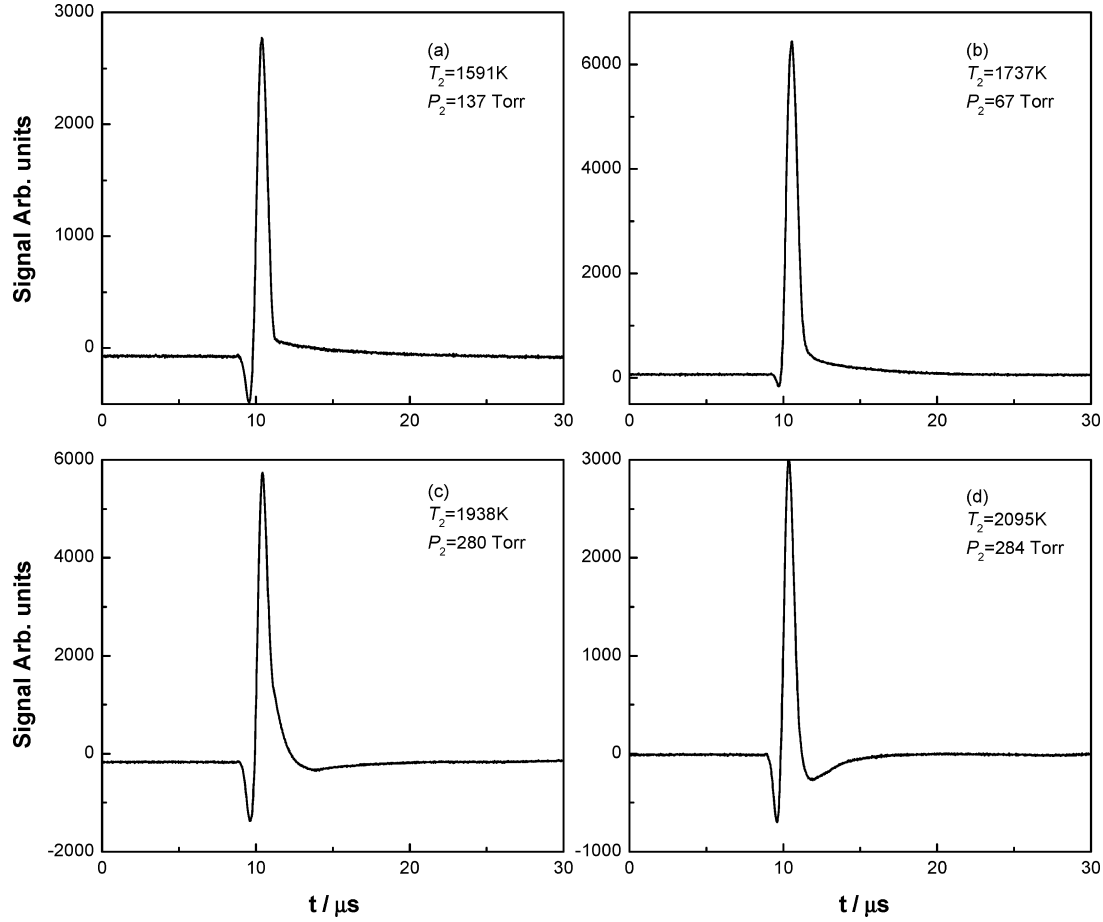

Figure 6. Example laser schlieren profiles for CH_3I decomposition experiments at various temperatures and pressures, (a and c) 2 and (b and d) 4% CH_3I/Kr.

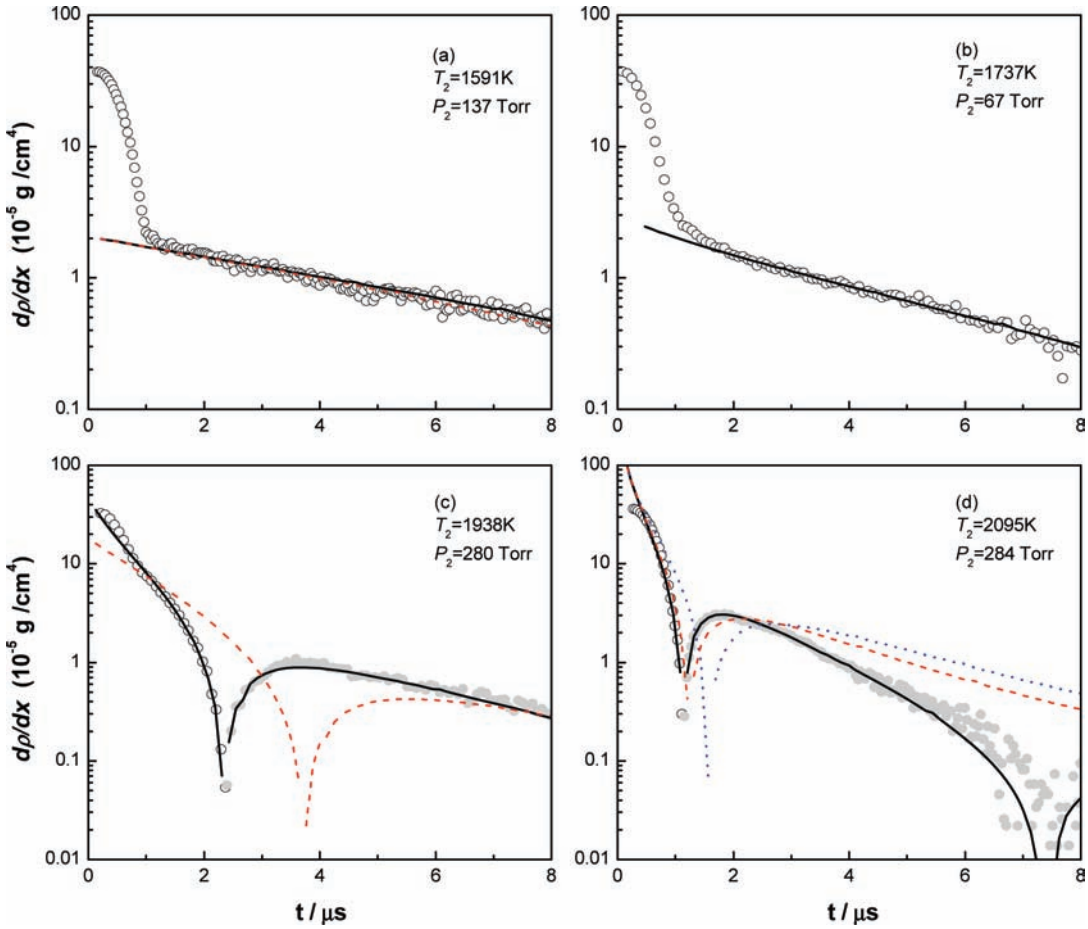

Figure 7. Example semilog plots of density gradients for the dissociation of CH_3I dilute in krypton. Absolute values are plotted. Experimental data: [○] represent positive values; [●] represent negative values. Simulation results using the mechanism listed in Table. 1 are represented by [—]; (a) 2% CH_3I, [red - - -] simulations with 14 step model (see text); (b) 4% CH_3I; (c) 2% CH_3I, [red - - -] Table 1 mechanism but with k_1 from ref 6; (d) 4% CH_3I [red - - -] simulations with the 14 step model (see text), [blue • • •] simulation with 14 step model + R_7, $CH_3I + H = CH_3 + HI$.

temperatures and pressures are much too high to resolve relaxation, and the signals following the spike are due to chemical reaction. Panels c and d of Figure 6 have an additional feature in the form of a valley following the shock front signal. Such valleys in LS signals are characteristic of strong exothermic processes.

In Figure 7, the first few falling points on each plot are due to the passage of the shock front through the laser beam, as before. The location of t_0, the point at which reaction starts, is obscured by the shock front, which is a ubiquitous problem with ST/LS experiments. However, methods for locating t_0 have been discussed in previous work,[33] and a well-established procedure is used that typically locates t_0 within 0.1−0.2 μs. The remaining points in the semilog plots represent the density gradient of interest. Rate coefficients for dissociation of the parent molecule are obtained by extrapolation of the density gradient profile back to t_0, where this is the sole reaction and $(d\rho/dx)_{t_0} \propto k_1$. For the lower-temperature experiments, this extrapolation is initially made, quite accurately, by inspection, and subsequently, the estimates are refined through simulation typically resulting in a <10% change in the initial estimates. For the higher-temperature experiments, determining the density gradient at t_0 is more difficult due to the steep slope of the early part of the data, and the initial rate coefficients are best determined through simulation of the complete LS profile by an iterative process, discussed later. However, even in these cases, the initial estimates rarely change by more than 10−20%.

The second-order rate coefficients for R_1 are shown in Figure 8a and compared to the existing literature data in Figure 8b along with the existing literature data from shock tube studies. There is very little scatter in the results from the current work, and the second-order values can be represented by the following expression over the range of 1500−2200 K

$$k_1 = 10^{50.626\pm0.037} T^{-9.52} \exp\left(\frac{-35962}{T}\right) \text{cm}^3\ \text{mol}^{-1}\ \text{s}^{-1}$$

The current results at 1600 K are about a factor of 1.3 higher than the CH_3 UV absorption results of Davidson et al.[4,7] and about 1.6 higher than the I-ARAS results of Kumaran et al.[6] While these differences are somewhat larger than desirable, the results of Davidson et al., Kumaran et al., and the current work are in reasonable agreement given the likely experimental errors.

In the present experiments, the most significant systematic error is the determination of t_0, which is generally most severe in the lower-pressure, low-temperature experiments due to greater curvature of the shock front. However, these experiments represent only a handful of the total set, and the profiles are very well simulated, yielding values for k_1 that are consistent with the higher-pressure and -temperature results. On the basis of the prior literature data, it has been assumed that CH_3I dissociates only by R_1 and is the sole contributor to the density gradient at t_0. If a secondary channel exists, then k_1 may be

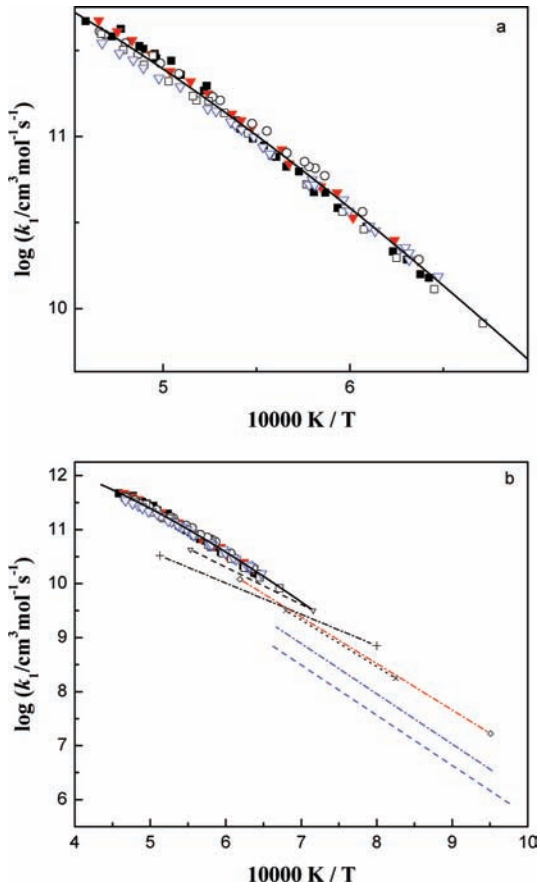

Figure 8. Arrhenius plot of second-order rate constants for $CH_3I \rightarrow CH_3 + I$ from laser schlieren experiments (a) and a comparison with the literature data (b); 4% CH_3I/Kr: P_2 = [■] 280, [red ▼] 146, and [○] 66 Torr; 2% CH_3I/Kr: P_2 = [□] 280 and [blue ▽] 146 Torr. The solid line is a least-squares fit (see text). [◇- - -◇] Kumaran et al.;[6] [▽- - -▽] Davidson et al.;[7] [+• • •+] Baeck et al.;[5] [×- - -×] Takahashi et al.[1] The blue lines represent the results of Saito et al., krypton bath gas [- - -][3] and argon bath gas [- • - • - •].[2]

overestimated. However, the two possibilities, elimination of HI and C−H fission, both have $\Delta H_{r,298}$ that are at least 50 kcal/mol higher than that of R_1 and can be excluded. For the C−H fission channel, the heat of reaction was estimated using 54.5 kcal/mol[34] as the heat of formation of CH_2I. Finally, in the lower-temperature experiments of the current work, secondary chemistry, discussed later, does not influence the determination of the density gradient at t_0, and in these experiments, estimation of k_1 at t_0 is straightforward. Consequently, as is evident from the following expression for the calculation of density gradients, the only remaining parameters that could influence the determination of k_1 are shock wave properties and thermochemical properties.

$$\frac{d\rho}{dx} = \frac{\rho\Sigma r(\Delta H - C_p T\Delta N)}{\rho_0 u(C_p T/M - C_v v^2/R)}$$

In the above expression r is the rate of reaction, ΔH the heat of reaction, ΔN the change in mole number, and the remaining quantities are just molecular heat capacities or incident shock parameters. The accuracy of the shock wave properties was addressed earlier, and variation of the thermochemical properties within the stated error bars[35] changed k_1 by only a few percent.

The first-order experimental rate constants for CH_3I dissociation were simulated with a restricted-rotor Gorin model RRKM

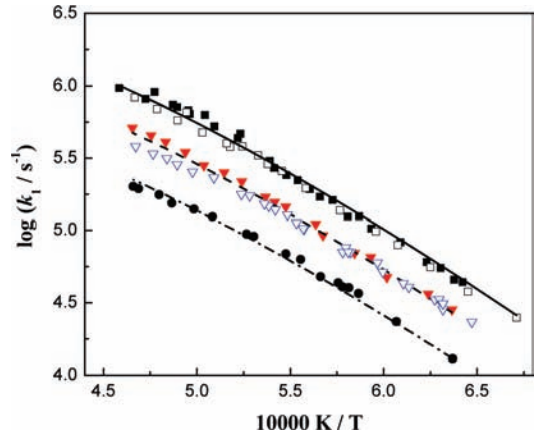

Figure 9. Arrhenius plots of the first-order rate constants for CH_3I at different pressures, 4% CH_3I/Kr at [■] 280, [red ▼] 146, and [●] 66 Torr and 2% CH_3I/Kr at [□] 280 and [blue ▽] 146 Torr. The lines represent RRKM calculations based on a restricted-rotor Gorin model with molecular parameters from Kumaran et al.[6] and $\langle\Delta E\rangle_{down} = 378 \times (T/298)^{0.457}$; [—] 280, [- - -] 146, and [- • - • - •] 66 Torr.

calculation. The molecular parameters, E_0, and hindrance parameter were taken from Kumaran et al.,[6] with the only exception being the collision energy between CH_3I and Kr, $\langle\Delta E\rangle_{down}$. As shown in Figure 9, the first-order rate constants are very well predicted with a temperature-dependent $\langle\Delta E\rangle_{down} = 378 \times (T/298)^{0.457}$ cm^{-1}. This has a similar temperature dependence as the collision energy determined from the vibrational relaxation experiments, but the absolute values are about 5−6 times larger. The difference between the $\langle\Delta E\rangle_{down}$ calculated from LS relaxation studies and that used in RRKM calculations has been seen in other LS studies and discussed therein; see, for example, ref 13. Kumaran et al. assumed a temperature-independent value for $\langle\Delta E\rangle_{down} = 590$ cm^{-1} which is about 200 cm^{-1} lower than the current value at 1600 K.

Simulation of Density Gradients. For all of the experiments with the exception of the lowest temperature, 66 Torr, ones, the early positive density gradients rapidly turn negative and reach a minimum before returning to the baseline at late time. This behavior is characteristic of an endothermic process being followed by an exothermic process, and the location of the transition from positive to negative gradients, the depth of the minimum, and the shape of the profile are all sensitive to the reaction mechanism and provide targets for mechanism development.

The density gradient profiles for all of the dissociation experiments were simulated using a computer code designed for reactive flows behind shock waves,[36] which also accounts for temperature changes due to reaction. Reverse reactions were included for all reactions through the equilibrium constant using thermodynamic data from Burcat and Russic.[35] An initial mechanism was constructed by simply adding R_1 to the ethane pyrolysis mechanism of Kiefer et al.[13] The reactions from the Kiefer et al. mechanism are indicated in Table 1, which contains the final mechanism from this work. During the initial simulations, all rate coefficients were fixed at the values used by Kiefer et al., with the exception of R_1.

At low reaction temperatures, this initial model provides a very good simulation of the experimental data, as shown in Figure 7a. However, at higher temperatures, the simulations fail to predict the experimental density gradients (Figure 7d, dashed red line), with the switch from positive to negative density gradients occurring later than observed experimentally and the overall shape of the profile being a poor fit to the experimental

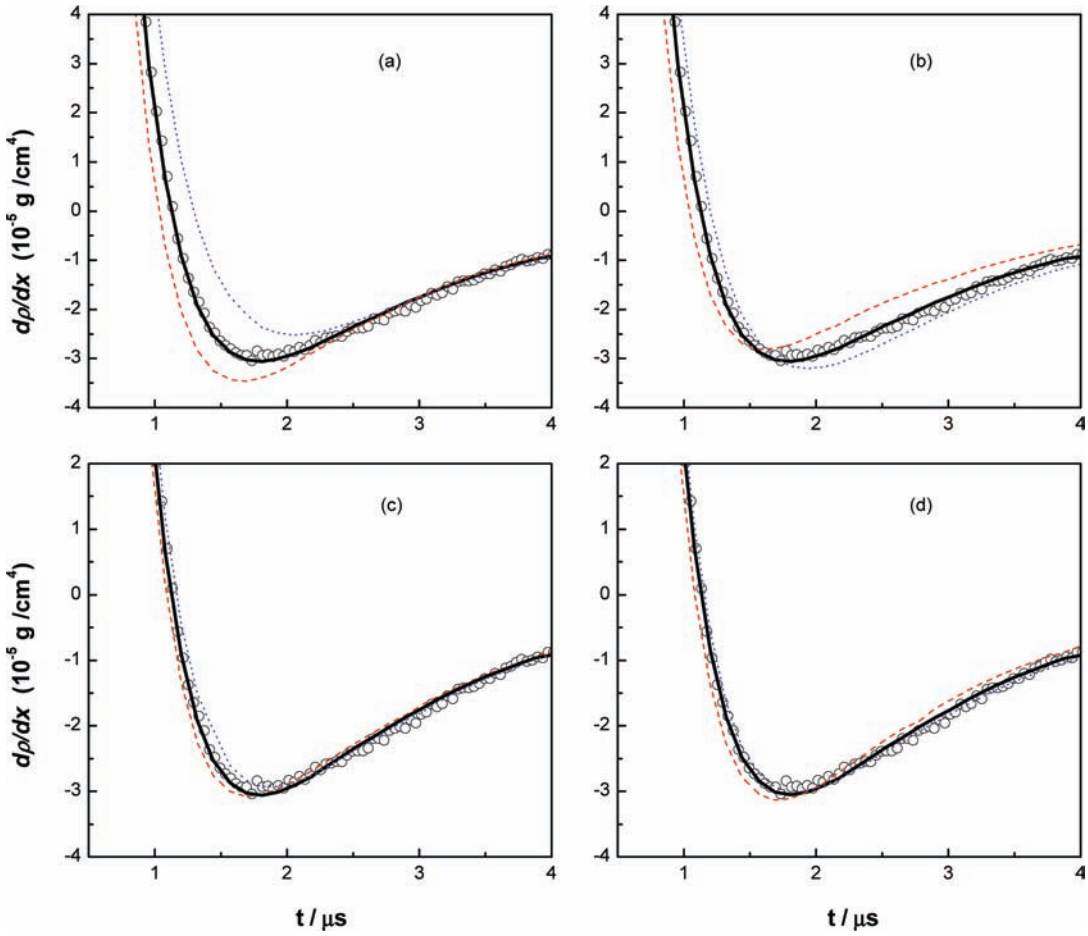

Figure 10. Examples showing the effect on the simulations of perturbations on various rate coefficients for the experiments shown in Figure 7d (P_2 = 284 Torr, T_2 = 2095 K, 4% CH_3I/Kr). Here, the abscissa has a linear scale unlike Figure 7d, where a log scale was used. The open circles [○] are the experimental values, and [—] are simulation results using the mechanism listed in Table 1 with the optimum rate constants; (a) [red - - -] $k_1 \times 1.2$, [blue • • •] $k_1 \times 0.8$; (b) [red - - -] $k_2 \times 2$, [blue • • •] $k_2 \times 0.5$; (c) [red - - -] $k_7 \times 2$, [• • •] $k_7 \times 0.5$; (d) [red - - -] $(k_4 + k_5) \times 2$, [• • •] $(k_4 + k_5) \times 0.5$.

data. Qualitatively, the prediction of experimental data also worsens with increasing pressure and reagent concentration.

Analysis of the low- and high-temperature simulations performed with the initial 14-step mechanism indicates the following: (a) In the low temperature regime, R_1 is dominant throughout the reaction period; (b) R_{-2}, methyl recombination to ethane (negative reaction numbers indicate the reverse reaction), contributes around one-third of the total density gradient after about 4 μs, with almost all of the remainder of the density gradient coming from R1; (c) also at 4 μs, R_3, $CH_3 + CH_3 \rightarrow C_2H_5 + H$, and R_{-6}, $C_2H_5 \rightarrow C_2H_4 + H$, start to contribute a few percent to the total density gradient. Consequently, the density gradient in the first few microseconds of reaction is entirely due to R_1 making assignment of k_1 at t_0 straightforward and accurate.

At high reaction temperatures, the situation is surprisingly not somewhat more complicated. Again, at early times, R_1 is effectively the only reaction occurring; however at about 0.5 μs, R_3 and R_{-6}, dissociation of C_2H_5, also make significant contributions to the positive density gradient. From 0.2 μs, R_{-2} starts to make negative contributions to the observed density gradient, with the maximum contribution at 2 μs, and the effect of R_{-2} tails after 4 μs as CH_3I and CH_3 radicals are consumed. At about 1 μs, the reactions of H-atoms with CH_3, R_{11}, and C_2H_3, R_{16}, also make large negative contributions to the density gradients. The remainder of the mechanism makes little or no contribution to the observed density gradient.

In contrast to the attempts to simulate the CH_3I experiments with the 14-step model, the Kiefer et al. mechanism accurately simulated their ethane dissociation LS experiments over a wide range of conditions that are similar to the current work. Furthermore, the experimental values for k_2 were accurately predicted by M.E. calculations from 70 to 5700 Torr, which included measurements of R_{-2} by CH_3 UV absorption.[13] Consequently, there is little reason to believe that the failure of the 14-step model to simulate the current high-temperature results is due to deficiencies in the rate coefficients of the initial model with the possible exception of R_1, dissociation of CH_3I. However, at low reaction temperatures, the 14-step model predicts the experimental density gradients very well, and altering k_1 by more than 10−15% would degrade the fit particularly in the first 1−2 μs. This is illustrated by the dashed line in Figure 7c, where k_1 from Kumaran et al.[6] replaced k_1 determined here in a simulation performed with the full mechanism, Table 1. While the simulation still hits the initial part of the experimental profile, the production of CH_3 radicals is far too slow. The simulation could be forced to provide a reasonable fit to the particular experiment shown in Figure 7c by increasing k_2 and adjusting other rate parameters. However, the changes required are not realistic and would not be applicable over the whole range of experiments. Furthermore, they would produce results that are incompatible with the ethane dissociation work of Kiefer et al. It is therefore most likely that the inability of the 14-step model to simulate the high-

temperature experimental data is due not to inaccuracies in rate coefficients but rather to missing reactions.

Of the possible channels for methyl recombination represented by R_{-2}, R_3, R_4, and R_5, only the first two appear in Kiefer's mechanism. While R_4 and R_5 would not contribute significantly to the density gradient due to their small heats of reaction, $\Delta H_{r,298K} = -5.5$ and $\Delta H_{r,298K} = -14.5$ kcal/mol, respectively, several of the subsequent reactions initiated by $^1CH_2$ and $^3CH_2$ would make significant contributions, Table 1. The results of simulations with the full mechanism in Table 1 and optimized values for, k_1, k_2, and k_7, discussed later, are shown in Figure 7a−d by the solid black lines, and the fit to the experimental results is very good.

At low reaction temperatures, analysis of the simulation results yields similar observations to those for the 14-step mechanism, with the primary difference being a small negative contribution from R_7, the attack of H atoms on CH_3I, which is initiated by the dissociation of C_2H_5, R_{-6}. The difference between the simulation results with the initial model and those with the full model are slight and only evident after about 6 μs in Figure 7a. At high temperatures, large negative contributions to the density gradient are made between 1 and 4 μs by R_{18}, $^3CH_2 + CH_3$, and R_7. R_{26} and R_{11} also make small negative contributions that affect mainly the late density gradient. Additionally, the importance of these bimolecular reactions varies somewhat with reagent concentration and reaction pressure.

In Figure 10, the sensitivity of the simulation to several parameters is demonstrated for the experiment shown in Figure 7d, where $T_2 = 2095$ K and $P_2 = 284$ Torr. In all of the sub figures, the solid black line represents the simulation results obtained with the optimized model, and the dashed and dotted lines represent perturbations of various rate coefficients. As shown in Figure 10a, the simulations are most sensitive to k_1, and a variation of only 20% has quite a dramatic effect. The location of the transition from positive to negative density gradients and the depth of the minimum are affected by both k_2 and k_7, Figure 10b and c, although these are rather more sensitive to k_2. However, as shown by the blue dotted line in Figure 7d, R_7 is an important addition to the to the initial 14-step reaction mechanism, and its inclusion makes a large improvement to the early part of the density gradient profile. Finally, the sequence of reactions involving methylene, especially R_{18}, that affect the late gradient are initiated by R_4 and R_5, the primary methylene-generating reactions. As discussed above, these two reactions do not contribute directly to the density gradient, but the sensitivity to perturbations in methylene concentration can be crudely tested by varying k_4 and k_5. As shown in Figure 10d, the mechanism shows little sensitivity to the reduced rate for these reactions, although doubling the rate does perturb the simulation somewhat.

The rate coefficient for reaction R_8, $C_2H_6 + H = C_2H_5 + H_2$, has been increased to the recommendation of Tsang and Hampson[37] from that estimated by Kiefer et al.[13] The effect is fairly small and mostly evident in the late profile as the density gradient recovers from the minimum toward the baseline. Overall, the increase in k_8 improves the curvature in this region across the whole experimental range.

In the final modeling, all rate coefficients, except those for R_1, R_2, and R_7, were fixed at literature values, and where appropriate, expressions were calculated for each reaction pressure from stated Troe parameters. In addition, incubation delays were accounted for by estimating incubation times from the collision energy, $\langle \Delta E \rangle_{down}$, obtained from the vibrational relaxation experiments and the method of Dove and Troe.[38] The estimated incubation times are about 1.8 μs for 20 Torr, in agreement with the observed incubation times 0.55 μs for 66 Torr, 0.22 μs for 146 Torr, and 0.1 μs for 280 Torr experiments. Figure 7b shows a low-pressure experiment where incubation has been incorporated into the simulation.

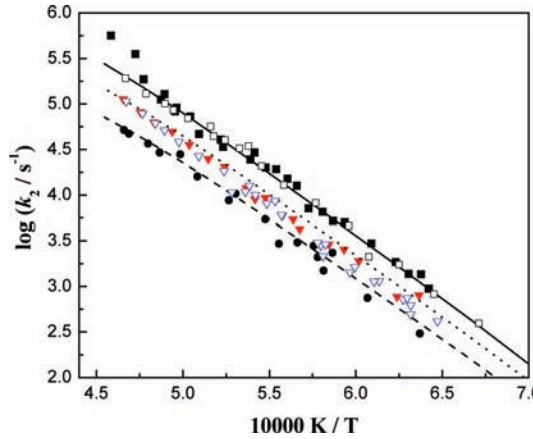

Figure 11. Arrhenius plots of the first-order rate constants for R_2 determined by fitting the CH_3I dissociation experiments; 4% CH_3I/Kr at [■] 280, [red ▼] 146, and [●] 66 Torr and 2% CH_3I/Kr at [□] 280 and [blue ▽] 146 Torr. The lines are results of RRKM calculations for [—] 280, [•••] 146, and [- - -] 66 Torr using the model of Kiefer et al.[13]

The location of the switch from positive to negative total density gradients and the depth of the minimum in the density gradient profile were quite sensitive to R_2. However, it was not necessary to vary the rate coefficient for this parameter by more than ±10% compared to that of Kiefer et al.[13] A comparison of the first-order rate coefficients at 66, 146, and 280 Torr from this work and the results of RRKM calculations from Kiefer et al. is shown in Figure 11. The bimolecular rate coefficients for R_2 from this work have been fitted with an Arrhenius expression.

$$k_2 = 10^{17.65\pm0.10} \exp\left(\frac{-32708}{T}\right) \text{cm}^3\ \text{mol}^{-1}\ \text{s}^{-1}$$

R_7 is the only reaction other than R_1 that removes CH_3I; R_{30} plays no role and mainly affects the curvature of the positive density gradient in the early part of the reaction. An Arrhenius expression has been fit to the bimolecular rate constants determined for R_7 over the temperature range of 1500−2000 K, and this is compared with the scant literature data in Figure 12.

$$k_7 = 10^{13.88\pm0.12} \exp\left(\frac{-601}{T}\right) \text{cm}^3\ \text{mol}^{-1}\ \text{s}^{-1}$$

The current results are a factor of 1.7 higher than an extrapolation of the experimental measurements of Yuan et al.[39] (flash photolysis resonance fluorescence at 295−757 K and 62−100 Torr) and about a factor of 3.5 lower than the theoretical predictions of Marshall et al.[40] Varying k_7 between these extremes requires only a small adjustment in k_1 to fit the early profile but forces large changes in other rate expressions to fit the remainder of the profile. These additional changes are not consistent across the experimental range and are also incompatible with the literature. Furthermore, introduction of R_7 into the 14-step mechanism produced a small improvement to the simulations of the high-temperature experiments by increasing

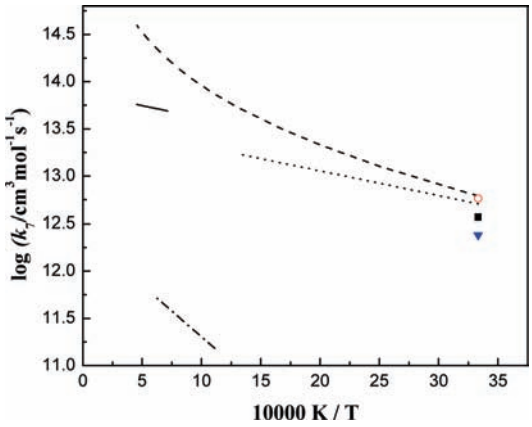

Figure 12. Comparison of the current estimates of bimolecular rate constants for R_7 and literature values; [—] this work; [• • •] Hynes et al.;[46] [- - -] Marshal et al.;[40] [- • - • - •] Yuan et al.;[39] [■] Sillesen et al.;[47] [red ○] Levy et al.;[48] and [blue ▼] Leipunskii et al.[49]

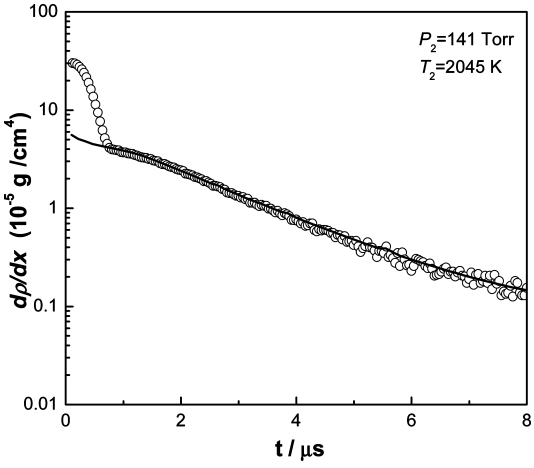

Figure 13. Semilog plot of laser schlieren density gradients from a dissociation experiment with 2% ethane dilute in krypton under conditions similar to those of Kiefer et al.[13] $T_2 = 2045$ K and $P_2 = 141$ Torr. The open circles [○] are experimental points, and the solid line [—] is the simulation with the mechanism in Table. 1.

consumption of CH_3I and producing methyl radicals; but by itself, it was not nearly sufficient.

The final mechanism presented in Table 1 simulated all of the dissociation experiments extremely well. The examples shown in Figure 7 span the whole experimental range of temperature, pressure, and concentration, and only minor adjustments of a few percent to R_1, R_2 and R_7 were needed to optimize the fit for each experiment.

In the current work, the methyl radical submechanism of Table 1 has been optimized to simulate the high-temperature self-reaction of methyl radicals. However, it should be equally capable of simulating the dissociation of ethane. To this end, we have repeated several of the ethane decomposition experiments of Kiefer et al.[13] and simulated the LS profiles with the mechanism in Table 1. An example is shown in Figure 13. Clearly, the agreement between simulation and experiment is superb.

Conclusion

The dissociation of CH_3I at high temperatures has been studied and a reaction mechanism developed that provides superb simulation of the complete set of 108 dissociation experiments over a broad range of reaction conditions and reagent concentrations. The reaction mechanism incorporates the formation of $^1CH_2$ and $^3CH_2$ via CH_3 recombination, and subsequent reactions are essential for simulation of the experiments in the higher-temperature range of the current work. In addition, the mechanism provides excellent simulations of ethane dissociation experiments at similar reaction conditions to the CH_3I dissociation. Consequently, we suggest that the mechanism here is a good high-temperature description of the pyrolytic reactions of methyl radicals.

Rate coefficients were determined for R_1, the dissociation of methyl iodide. The values are self-consistent over the entire experimental range but lie about a factor of 1.3−1.6 higher at 1600 K than previous studies using ARAS and UV absorption. On the basis of consideration of potential sources of error in the current work and the success of the modeling effort, the difference cannot be reconciled. The first-order rate coefficients from the current work are very well simulated by RRKM calculations based on a model by Kumaran et al.[6] but with a larger temperature-dependent energy-transfer parameter.

Finally, vibrational relaxation was observed in CH_3I at low reaction pressures and a wide range of temperatures. From some of these experiments, incubation times were also obtained and used to estimate incubation delays in the dissociation experiments.

Thus, a solid mechanism has been developed that simulates the LS profiles associated with CH_3I dissociation and accurately describes the secondary chemistry, which achieves the initial goal of characterizing CH_3I as a methyl radical source in high-concentration environments.

Acknowledgment. This work was performed under the auspices of the Office of Basic Energy Sciences, Division of Chemical Sciences, Geosciences, and Biosciences, U.S. Department of Energy, under contract number DE-AC02-06CH11357. C.F.G. also wishes to acknowledge support from the National Science Foundation under the Graduate Research Fellowship Program. We would like to thank John H. Kiefer for many interesting discussions concerning this work and Lawrence B. Harding and Stephen J. Klippenstein for discussion of the methylene-forming reactions.

Supporting Information Available: A table containing the T_2, P_2, τ_{app}, $P\tau$, $\rho(\infty) - \rho(0)$, and $\Delta\rho$(experimental)/$\Delta\rho$(thermo) is available. A table containing the initial and final conditions for the dissociation experiments and values of k_1 and k_2 is also available. This material is available free of charge via the Internet at http://pubs.acs.org.

References and Notes

(1) Takahashi, K; Inoue, A.; Inomata, T. In *Shock Waves Proceedings of the 20th*; International Symposium on Shock Waves, Pasadena, USA, July 1995. (a) Sturtevant, B., Shepard, J. E., Hornung, H. G., Eds.; World Scientific Publishing Co. Pte. Ltd.: Singapore, 1996; pp 959−964.

(2) Saito, K.; Tahara, H.; Murakami, I. *Bull. Chem. Soc. Jpn.* **1984**, *57* (10), 3023–3024.

(3) Saito, K.; Tahara, H.; Kondo, O.; Yokubo, T.; Higashihara, T.; Murakami, I. *Bull. Chem. Soc. Jpn.* **1980**, *53* (5), 1335–1339.

(4) Davidson, D. F.; Chang, A. Y.; Dirosa, M. D.; Hanson, R. K. *J. Quant. Spectrosc. Radiat. Trans.* **1993**, *49* (5), 559–571.

(5) Baeck, H. J.; Shin, K. S.; Yang, H.; Qin, Z.; Lissianski, V.; Gardiner, W. C. *J. Phys. Chem.* **1995**, *99* (43), 15925–15929.

(6) Kumaran, S. S.; Su, M. C.; Michael, J. V. *Int. J. Chem. Kinet.* **1997**, *29* (7), 535–543.

(7) Davidson, D. F.; Dirosa, M. D.; Chang, E. J.; Hanson, R. K.; Bowman, C. T. *Int. J. Chem. Kinet.* **1995**, *27* (12), 1179–1196.

(8) Ogg, R. A. *J. Am. Chem. Soc.* **1934**, *56* (3), 526–536.

(9) Kodama, S.; Ooi, Y. *Bull. Chem. Soc. Jpn.* **1990**, *63* (3), 877–885.

(10) Butler, E. T.; Polanyi, M. *Trans. Faraday Soc.* **1943**, *39*, 0019−0035.

(11) Horrex, C.; Lapage, R. *Discuss. Faraday Soc.* **1951**, *10*, 233–234.

(12) Manion, J. A.; Huie, R. E.; Levin, R. D. ; Burgess, D. R., Jr.; Orkin, V. L.; Tsang, W.; McGivern, W. S.; Hudgens, J. W.; Knyazev, V. D.; Atkinson, D. B.; Chai, E.; Tereza, A. M.; Lin, C.-Y.; Allinson, T. C.; Mallard, W. G.; Westley, J. T.; Herron, J. T.; Hampson, R. F.; Frizzell, D. H. *NIST Chemical Kinetics Database*, NIST Standard Reference Database 17, Version 7.0 (Web Version), Release 1.4.2, Data version 2008.12; National Institute of Standards and technology: Gaithersburg, MD, 2008; http://kinetics.nist.gov.

(13) Kiefer, J. H.; Santhanam, S.; Srinivasan, N. K.; Tranter, R. S.; Klippenstein, S. J.; Oehlschlaeger, M. A. *Proc. Combust. Inst.* **2005**, *30*, 1129–1135.

(14) Oehlschlaeger, M. A.; Davidson, D. F.; Hanson, R. K. *Proc. Combust. Inst.* **2005**, *30*, 1119–1127.

(15) Lim, K. P.; Michael, J. V. *Proc. Combust. Inst.* **1994**, *25*, 713–719.

(16) Stewart, P. H.; Larson, C. W.; Golden, D. M. *Combust. Flame* **1989**, *75* (1), 25–31.

(17) Frank P.; Braun-Unkhoff, M. In *Shock Tubes and Waves*; Proceedings of the 16th International Symposium on Shock Tubes and Waves, Aachen, West Germany, July 26-31, 1987; Groenig H., Ed.; VCH: Weinheim, Germany, 1988; pp 379−385.

(18) Roth, P. *Forsch. Ingenieurwes.* **1980**, *46*, 93–102.

(19) Bohland, T.; Dobe, S.; Temps, F.; Wagner, H. G. *Ber. Bunsen-Ges. Phys. Chem.* **1985**, *89*, 1110–1116.

(20) Jasper, A. W.; Klippenstein, S. J.; Harding, L. B. *J. Phys. Chem. A* **2007**, *111* (35), 8699–8707.

(21) Saxena, S.; Kiefer, J. H.; Tranter, R. S. *J. Phys. Chem. A* **2007**, *111* (19), 3884–3890.

(22) Kiefer, J. H.; Sahukar, G. C.; Santhanam, S.; Srinivasan, N. K.; Tranter, R. S. *J. Chem. Phys.* **2004**, *120* (2), 918–925.

(23) Santhanam, S.; Kiefer, J. H.; Tranter, R. S.; Srinivasan, N. K. *Int. J. Chem. Kinet.* **2003**, *35* (8), 381–390.

(24) Tranter, R. S.; Giri, B. R. *Rev. Sci. Instrum.* **2008**, *79* (9), 094103.

(25) Kiefer, J. H. The Laser Schlieren Technique in Shock Tube Kinetics. In *Shock Waves in Chemistry*; Lifshitz, A. , Ed.; Marcel Dekker: New York, 1981; pp 219−277.

(26) Kiefer, J. H.; Alalami, M. Z.; Hajduk, J. C. *Appl. Opt.* **1981**, *20* (2), 221–230.

(27) Gardiner, W. C.; Hidaka, Y.; Tanzawa, T. *Combust. Flame* **1981**, *40* (2), 213–219.

(28) Cottrell, T. L.; McCoubrey, J. C. *Molecular Energy Transfer in Gases*; Butterworths: London, 1961.

(29) Blythe, P. A. *J. Fluid Mech.* **1961**, *10*, 33–47.

(30) Kiefer, J. H.; Kumaran, S. S.; Sundaram, S. *J. Chem. Phys.* **1993**, *99* (5), 3531–3541.

(31) Fogg, P. G. T.; Hanks, P. A.; Lambert, J. D. *Proc. R. Soc. London, Ser. A* **1953**, *219* (1139), 490–499.

(32) Srinivasan, N. K.; Kiefer, J. H.; Tranter, R. S. *J. Phys. Chem. A* **2003**, *107* (10), 1532–1539.

(33) Kiefer, J. H.; Manson, A. C. *Rev. Sci. Instrum.* **1981**, *52* (9), 1392–1396.

(34) Seetula, J. A. *Phys. Chem. Chem. Phys.* **2002**, *4* (3), 455–460.

(35) Burcat, A.; Ruscic, B. Gas Thermochemical Database with updates from Active Thermochemical Tables; ftp://ftp.technion.ac.il/pub/supported/aetdd/thermodynamics (Accessed April, 10 2009); mirrored athttp://garfield.chem.elte.hu/Burcat/burcat.html (Accessed April, 10 2009).

(36) Gardiner, W. C.; Walker B. F.; Wakefield C. B. Mathematical Methods for Modelling Chemical Reactions. In *Shock Waves in Chemistry*; Lifshitz, A. , Ed.; Marcel Dekker Inc.: New York, 1981; pp 319−374.

(37) Tsang, W.; Hampson, R. F. *J. Phys. Chem. Ref. Data* **1986**, *15* (3), 1087–1279.

(38) Dove, J. E.; Troe, J. *Chem. Phys.* **1978**, *35* (1−2), 1–21.

(39) Yuan, J.; Wells, L.; Marshall, P. *J. Phys. Chem. A* **1997**, *101* (19), 3542–3546.

(40) Marshall, P.; Misra, A.; Berry, R. J. *Chem. Phys. Lett.* **1997**, *265* (1−2), 48–54.

(41) Miller, J. A.; Klippenstein, S. J. *Phys. Chem. Chem. Phys.* **2004**, *6* (6), 1192–1202.

(42) Baulch, D. L.; Bowman, C. T.; Cobos, C. J.; Cox, R. A.; Just, T.; Kerr, J. A.; Pilling, M. J.; Stocker, D.; Troe, J.; Tsang, W.; Walker, R. W.; Warnatz, J. *J. Phys. Chem. Ref. Data* **2005**, *34* (3), 757–1397.

(43) Sutherland, J. W.; Su, M. C.; Michael, J. V. *Int. J. Chem. Kinet* **2001**, *33* (11), 669–684.

(44) Alalami, M. Z.; Kiefer, J. H. *J. Phys. Chem.* **1983**, *87* (3), 499–506.

(45) Saito, K.; Tahara, H.; Kondo, O.; Yokubu, T.; Thigashihara, T.; Murakami, I. *Bull. Chem. Soc. Jpn.* **1980**, *53*, 1335–1339.

(46) Hynes, R. G.; Mackie, J. C.; Masri, A. R. *Proc. Combust. Inst* **2000**, *28*, 1557–1562.

(47) Sillesen, A.; Ratajczak, E.; Pagsberg, P. *Chem. Phys. Lett.* **1993**, *201* (1−4), 171–177.

(48) Levy, M. R.; Simons, J. P. *J. Chem. Soc., Faraday Trans. 2* **1975**, *71*, 561–570.

(49) Leipunskii, I. O.; Morozov, I. I.; Tal'roze, V. L. *Dokl. Phys. Chem. (Engl. Transl.)* **1971**, *198*, 547–550.

JP903336U